Modelling the solid–liquid–vapour phase behaviour of *n*-alkanes in a TPT-1 framework

Viridiana Ramírez-Carpio[a], Amparo Galindo[b], Alejandro Gil-Villegas[a]

[a]División de Ciencias e Ingenierías, Campus León, Universidad de Guanajuato, Lomas del Bosque 103, León, Guanajuato, 37520, Mexico; [b]Department of Chemical Engineering, Institute of Molecular Science and Engineering, Imperial College London, South Kensington Campus, SW7 2AZ, UK.

ARTICLE HISTORY
Compiled April 13, 2023

ABSTRACT
We study the global phase behaviour of *n*-alkanes applying Wertheim's first order thermodynamic perturbation theory (TPT1). The molecules are modelled as homonuclear chains comprised of *m* freely jointed spherical segments interacting via the Lennard-Jones potential. Vega *et al.* [J. Chem. Phys. 116, 17 (2002)] have shown that the TPT1 is suitable to treat solid phases as well as fluid phases when model chains are considered, but that the adoption of a fully flexible chain model leads to the under-prediction of triple point temperatures and overestimation of the fluid ranges in comparison to experiment. Here, we propose a model in which a different number of segments are used to treat the fluid and the solid phase. The number of segments used to model the molecules in the fluid phase m_f, and the LJ monomer potential parameters σ and ε are taken from published soft-SAFT values, whereas in the case of the solid phase a reduced temperature-dependent effective chain length $m_s(T^*)$ is determined through a minimisation between theoretical and experimental liquid-solid phase equilibrium data. We refer to this model as effective-solid TPT1 (es-TPT1). We use the model proposed to calculate the solid–liquid–vapour phase diagrams of several *n*-alkanes and compare with experimental data. In the approach proposed, the conformation of chains in the solid phase is decoupled from the fluid phase, and an excellent description of the melting properties, as well as accurate predictions of the triple point temperatures for the *n*-alkanes examined is obtained. This simple solution provides an avenue to model the solid–liquid–vapour phase behaviour of other real substances in a TPT1 framework, and hence within the SAFT family of equations.

KEYWORDS
n-alkanes, phase behaviour, solid–liquid equilibrium, TPT1

1. Introduction

The thermodynamic properties and phase behaviour of *n*-alkanes are directly relevant in diverse scientific and industrial areas. The oil and chemical industries are rich in processes that involve multicomponent fuel, oil, and wax fluid mixtures [1], which are employed in the manufacturing of consumer goods and cosmetics [2, 3], while in flow assurance, the prevention of wax precipitation in pipelines and refinery equipment [4–6] requires an ability to identify the appearance of solid phases. *N*-alkanes and their blends are also of current interest as latent heat energy storage (LHES) materials, for their high latent heats, stable phase change and high enthalpies, that can greatly improve wind and solar energy storage [7, 8]. They also

CONTACT Alejandro Gil-Villegas. Email: gil@fisica.ugto.mx

serve as model compounds to glean insights into the non-polar driving forces of biologically related mechanisms in protein folding and binding, given the aliphatic content many amino acid side chains [9, 10], in controlling lipid self-assembly and micelle formation [11, 12], in agriculture where the phase behaviour and deposition of long-chain *n*-alkanes on the surfaces of plants is of interest [13, 14] and in paleovegetation studies [15] where the distribution pattern of *n*-alkanes across chain lengths is used as a biomarker to determine past vegetation species.

From a theoretical perspective, the development of predictive models is relevant to the study of the impact of size and conformation of chain molecules on the resulting macroscopic thermodynamic properties. Several models have been proposed over the years to study the solid–fluid equilibrium of chain molecules using computer simulations. An excellent review relating to model systems was presented by Monson and Kofke [16]. Malanoski and Monson [17, 18] also determined the solid–fluid equilibrium of freely jointed hard sphere chains and presented models of *n*-alkanes to study their solid–fluid phase equilibrium using computer simulations. They noted that although changes in molecular shape lead to deviations from the principle of corresponding states in both vapor–liquid and solid–liquid equilibrium, the effects in the latter were substantially larger [17]. Polson and Frenkel [19] examined the solid–fluid equilibrium of tangent-sphere chain models implementing Lennard-Jones rather than hard-sphere interactions and incorporating bond stretching and bond bending potentials to limit the molecular flexibility.

There is a vast literature related to the development of computer simulation force-fields, from atomistic to coarse-grain models [20–26]. In terms of modelling the *n*-alkanes, one of the most successful has been the transferable potentials for phase equilibria united-atom (TraPPE-UA) [26], in which CH_x groups are represented as single interaction sites placed on the carbon atoms, with bond lengths, angles and force constants included. There are many molecular dynamics (MD) and Monte Carlo (MC) simulation studies on the liquid–vapour, interfacial properties, and surface tension of *n*-alkanes [27–31]. With reference to solid–liquid equilibrium (SLE), all-atom force fields have been re-parameterised to reproduce both fluid and solid properties [32, 33] of long alkanes. Burrows *et al.* [34] determined the SLE via computer simulation using several force fields predicting the melting point and order-parameter values in order to identify crystal-rotator phase transitions for *n*-pentadecane and *n*-hexadecane.

Experimental works on the SLE of *n*-alkanes have also been reported by several authors. Würflinger and coworkers [35–37] determined the solid–liquid transitions of *n*-alkanes using differential thermal analysis (DTA) at high pressure, reporting DTA thermograms and $P-T$ melting curves. Hohne *et al.* [38] have used high-pressure differential scanning calorimetry (DSC) to obtain the variation of heat flow with temperature in the solid−liquid coexistence line. Pauly *et al.* [39], Morawski *et al.* [40] and Domańska *et al.* [41, 42] have obtained melting curves at high pressure for both pure *n*-alkanes and waxy mixture systems using the synthetic method that involves the visual observation of phase transition boundaries. Other authors, such as Tanaka *et al.* [43], Daridon *et al.* [44], Machado *et al.* [45], Nelson *et al.* [46] and Milhet *et al.* [47] have used the thaw–melt method and polarizing microscope to determine visually SLE temperatures. All these works report the temperatures of the solid–liquid transition as function of the pressure in $P-T$ curves for some *n*-alkanes and cycloalkanes, within a range of 1-3000 bars.

In terms of theoretical methods, a range of approaches for chain systems have been developed following statistical mechanical approaches. For example, within the lattice-model family, the Flory-Huggins [48, 49], generalized Flory (GF) [50], and generalized Flory-dimer (GF-D) [51] equations of state, each with increasing accuracy have been presented. Lattice models account for both the volume occupied by the monomer units on the chain molecules

and the large number of configurations available for long flexible chains. Concentrated polymer solutions, melts, and blends are systems often described using Flory-Huggins lattice theories. Coutinho *et al.* [52] found that the Flory free-volume theory is an acceptable model for the description of a liquid mixture of saturated hydrocarbons in equilibrium with a solid phase. They also studied the solid–liquid equilibrium of *n*-alkanes using the chain delta lattice parameter model (CDLP) [53], valid up to 100 bar.

The first-order thermodynamic perturbation theory (TPT1) proposed by Wertheim [54–59] was used by Chapman *et al.* [60, 61] to develop the statistical associating fluid theory (SAFT) to predict the thermodynamic properties of fluids of associating chain molecules, using as reference system the hard-sphere fluid. Variations of the SAFT equation introduce improvements in the way the pair-potentials or the structural properties of the system are determined [62–67]. The resulting EOSs from this formalism are very useful, as they describe and predict the thermodynamic properties of chain fluids very accurately [68–73]. In the TPT1 approach, the Helmholtz free energy of the chain system is obtained from the Helmholtz free energy and contact pair correlation function of a corresponding monomer system at the same density and temperature. Johnson *et al.* [74] demonstrated that Wertheim's formalism yields a good description of the fluid properties of freely jointed tangent Lennard-Jones chain molecules, and its soft-SAFT [64, 65] extension has been used very successfully to model the properties of real fluid mixtures.

In terms of treating the solid phase, Vega and MacDowell [75] found that Wertheim's TPT1 can be extended to the solid phase of freely jointed hard spheres, obtaining excellent agreement with the simulation results of Malanoski and Monson [17]. In a later work, Vega *et al.* [76] extended Wertheim's TPT1 approach in order to obtain the solid phase and solid–liquid-vapour phase behaviour of freely jointed Lennard-Jones molecules, using the van der Hoef equation of state [77] for the solid phase and structural information from computer simulation data. The theory, when applied to dimers, is in excellent agreement with computer simulation values of the fluid-fluid and fluid-solid boundaries, including the triple point. For longer chains, the infinite-chain limits are qualitatively reproduced although the predicted triple-point temperature variations with chain length are small, which results in very large fluid ranges. As an example, while the ratio of the triple point temperature to the critical temperature ($T_{\rm tr}/T_{\rm c}$) in polyethylene is reported experimentally as 0.4 [78], the theoretical approach leads to a value of 0.14. This result suggests that although a fully-flexible tangent-bead model can be suitable to treat the fluid phase behavior of chain molecules this is not the case for the solid phase. Blas *et al.* [79] determined the vapour–liquid–solid phase diagrams of flexible hard-sphere chains by adding a mean-field term in order to account for attractive dispersion forces, and later studied the global phase behavior of linear rigid tangent hard-sphere chains [80]. For the case of LJ chain molecules, a comparison between rigid linear and flexible molecules of tangent segments was presented in a later work showing that the triple-point temperature of linear rigid LJ chains increases dramatically with chain length [81].

The fully-flexible model allows the existence of a singular solid of ordered segments but disordered bonds, which is not realistic when describing real molecules. The existence of bond angles and torsional potentials means that such a high-density solid cannot be observed. In order to improve the TPT1 description of the fluid–solid phase boundaries to treat real molecules, we propose a model in which the fluid and solid phases are treated with different values of the numbers of segments m in the chain-molecule model. The soft-SAFT model [64, 65] is used to treat the fluid phases, while a different temperature-dependent value of m is determined for the solid phases. The same molecular model is needed to treat vapour and liquid phases given the existence of fluid–fluid critical points (in pure compounds and mixtures). However, a separate model can be proposed to treat the solid phase as there is

no fluid–solid critical point at any condition (no continuous transition is possible between a positionally disordered phase and an ordered one). As shown later, a very good description of the fluid–solid phase boundaries for a range of *n*-alkanes is obtained with the approach proposed. The theoretical framework and models used in the current work are presented in Section 2; results and discussion are presented in Section 3; conclusions are given in Section 4.

2. Theory and molecular models

We present the main ideas in Wertheim's TPT1 by following the formulation introduced by Zhou and Stell [82]. We consider a system of N^{ref} spherical monomer particles contained within a volume V at temperature T, interacting via the Lennard-Jones pair potential u^{ref},

$$u^{\text{ref}}(r) = 4\varepsilon\left[\left(\frac{\sigma}{r}\right)^{12} - \left(\frac{\sigma}{r}\right)^{6}\right], \tag{1}$$

where r is the centre-centre distance between two particles, σ is the distance at which the potential is zero, and ε is the well-depth energy of the potential. We denote this system as the reference system, with its properties labeled with the superscript 'ref' throughout. The reduced number density of this system is $\rho^{\text{ref}} = N^{\text{ref}}\sigma^3/V$. Let us also assume that in another container of volume V and temperature T there is a number N of fully flexible chain molecules. The reduced density of the chain system is $\rho = N\sigma^3/V$. Each chain consists of m spherical monomers, with a fixed bond length $L = \sigma$, and by fully flexible chains we mean that there are no constraints in either angle bending or torsion. The reference and chain systems are related by $N = N^{\text{ref}}/m$ and $\rho = \rho^{\text{ref}}/m$.

The Helmholtz free energy A of the chain system is given by [60, 83]

$$\frac{A}{NkT} = \frac{A^{\text{ideal}}}{NkT} + \frac{A^{\text{mono}}}{NkT} + \frac{A^{\text{chain}}}{NkT}, \tag{2}$$

where k is the Boltzmann constant, A^{ideal} is the ideal free energy, A^{mono} is the residual free energy due to the interactions between monomer segments, and A^{chain} is the contribution due to the formation of chains of monomers. The ideal contribution to the Helmholtz free energy of the chain system is given as

$$\frac{A^{\text{ideal}}}{NkT} = \ln(\rho\Lambda^3) - 1, \tag{3}$$

where Λ represents the de Broglie thermal wavelength. The monomer free-energy contribution is given by

$$\frac{A^{\text{mono}}}{NkT} = \frac{A^{\text{ref}}_{\text{residual}}}{NkT}, \tag{4}$$

where $A^{\text{ref}}_{\text{residual}}$ is the residual free energy of the reference system. The corresponding contribution due to the formation of chain molecules is given by

$$\frac{A^{\text{chain}}}{NkT} = -(m-1)\ln y^{\text{ref}}(\sigma), \tag{5}$$

where $y^{\text{ref}}(\sigma)$ is the background correlation function of the reference monomer system at contact length. This function is related to the radial distribution function $g^{\text{ref}}(r)$ by

$$y^{\text{ref}}(r) = \exp[\beta u^{\text{ref}}(r)] g^{\text{ref}}(r), \tag{6}$$

where $\beta = 1/kT$. Since the LJ potential is equal to zero at $r = \sigma$, $y^{\text{ref}}(\sigma) = g^{\text{ref}}(\sigma)$. Therefore, we can write

$$\frac{A^{\text{chain}}}{NkT} = -(m-1)\ln g^{\text{ref}}(\sigma). \tag{7}$$

Thus, if the residual free energy of the reference system and its pair radial distribution function at contact length are known, equations (3), (4) and (7) provide the free energy of the chain system. This formalism is not restricted to a fluid system and can also be applied to describe solid phases [75].

The corresponding equation of state is given as

$$Z = mZ^{\text{ref}} - (m-1)\left(1 + \rho^{\text{ref}} \frac{\partial \ln g^{\text{ref}}(\sigma)}{\partial \rho^{\text{ref}}}\right), \tag{8}$$

where Z and Z^{ref} are the compressibility factors of the chain and reference system, respectively. The chemical potential is obtained from the Helmholtz free energy by differentiation as

$$\frac{\mu}{kT} = \left(\frac{\partial (A/kT)}{\partial N}\right)_{T,V}. \tag{9}$$

Fluid Phase. The Helmholtz free energy of the chain system in the fluid phase is given by

$$\frac{A_{\text{f}}}{NkT} = \frac{A^{\text{ideal}}}{NkT} + \frac{A^{\text{ref}}_{\text{residual,f}}}{NkT} - (m_{\text{f}} - 1)\ln g^{\text{ref}}_{\text{f}}(\sigma), \tag{10}$$

where m_{f} is the number of monomers in the model fluid chain, and the subscript f refers to properties of a fluid state. The residual free energy and radial distribution function of the LJ monomer fluid are given by the expressions provided by Johnson et al. [74, 84].

Solid Phase. Following Vega and MacDowell [75], the Helmholtz free energy of the solid chain system is written as,

$$\frac{A_{\text{s}}}{NkT} = \frac{A^{\text{ideal}}}{NkT} + \frac{A^{\text{ref}}_{\text{residual,s}}}{NkT} - (m_{\text{s}}(T^*) - 1)\ln g^{\text{ref}}_{\text{s}}(\sigma) \tag{11}$$

where the free energy of the reference monomer solid systems is given by the van der Hoef EOS [77] and the contact value of the radial distribution function of the reference solid is obtained from computer simulations [76]. In the current work, a temperature dependence is introduced in the parameter m_{s} that describes the number of segments in the chain in the solid phase.

Calculation of phase equilibrium. The conditions of phase equilibrium, given by [85]

$$\begin{aligned} T^{\mathrm{I}} &= T^{\mathrm{II}} \\ P^{\mathrm{I}} &= P^{\mathrm{II}} \\ \mu^{\mathrm{I}} &= \mu^{\mathrm{II}} \end{aligned} \tag{12}$$

are solved using a standard Newton-Raphson method [86]. The subscripts I and II refer to the phases involved in the equilibrium, and $P = Z\rho kT$ is the pressure.

Models. We select a number of *n*-alkanes for which experimental data of the solid–fluid phase boundaries are available [35–47].

Fluid phases (liquid and vapour) are modelled using the soft-SAFT molecular parameters (σ, ε/k and m_{f}), which have been shown to provide an accurate description of the fluid phase behaviour for *n*-alkanes [87, 88]. For completeness, we provide the parameters of the relevant *n*-alkanes in Table 1.

Table 1. Soft-SAFT fluid-phase molecular parameters for the selected *n*-alkanes [87, 88]: σ denotes the segment diameter, ε the well-depth energy and m_{f} the number of segments in the fluid chain model.

n-alkane	σ / Å	(ε/k) / K	m_{f}
C7	3.9498	260.31	3.1834
C8	3.9632	265.23	3.5381
C9	3.9740	269.30	3.8971
C12	3.9971	277.97	4.9715
C13	4.0026	280.08	5.3294
C15	4.0118	283.55	6.0447
C16	4.0156	284.99	6.4015
C17	4.0189	286.29	6.7600
C18	4.0220	287.45	7.1176
C24	4.0352	292.54	9.2636

Two theoretical models are considered for the solid phase: a model in which number of segments used to model the molecules is the same as in the fluid phase (i.e., $m_{\mathrm{s}} = m_{\mathrm{f}}$, with the values provided in Table 1), and a new model in which a different number of segments is used to model the solid phase $m_{\mathrm{s}} \neq m_{\mathrm{f}}$. We refer to the first model as TPT1 and to our new model as effective-solid TPT1 (es-TPT1).

In the es-TPT1 model, in order to provide an accurate description of the fluid-solid phase boundaries and the triple point temperature of the *n*-alkanes, a parameter m_{s}, function of temperature, is incorporated. Using experimental pressure and temperature data along the melting line an objective function

$$F_{\mathrm{Obj}} = \left(\frac{P^{\mathrm{exp}}_{\mathrm{melting}} - P^{\mathrm{calc}}_{\mathrm{melting}}(\Theta)}{P^{\mathrm{exp}}_{\mathrm{melting}}} \right)^2, \tag{13}$$

where Θ is the vector of model parameters of the fluid and solid phases and P_{melting} the melting pressure (calculated and experimental, as indicated by the superscripts, calc and exp, respectively) is minimised in order to determine the optimal value of m_{s} at each temperature. In this way, a unique value of m_{s} is obtained for each experimental melting point along the liquid-solid $P-T$ coexistence line. For each of the *n*-alkanes considered, an analytical expression for m_{s} as function of temperature, is obtained carrying out least-square fit using a

rational function given as

$$m_{\rm s}(T^*) = \frac{a_0 + a_1 T^* + a_2 T^{*2}}{1 + a_3 + a_4 T^* + a_5 T^{*2}}, \tag{14}$$

in a similar vein to previous work [89], where $T^* = kT/\varepsilon$ is a reduced temperature. The coefficients a_i are given in Table 2.

Table 2. Least-square fit coefficients for the rational function parametrisation of $m_{\rm s}$ as a function of temperature, cf. Eq.(14).

n-alkane	a_1	a_2	a_3	a_4	a_5
C7	-3.55540	-15.00640	25.42650	-10.22460	11.57330
C8	3.26514	-9.71677	9.32202	-3.13325	2.94599
C9	3.67436	-9.38873	6.36598	-2.57531	1.74467
C12	2.92552	-9.96878	6.85490	-2.73535	1.70075
C13	9.70801	-53.54620	69.43590	-11.04090	14.43030
C15	4.24310	-12.4662	8.39720	-2.61062	1.63539
C16	5.92174	-12.73076	6.79172	-2.11036	1.10810
C17	-1.88632	-89.5700	107.67200	-16.20290	17.29400
C18	5.68992	-70.1648	89.92970	-12.48460	14.3900
C24	-13.76820	-52.9523	68.73750	-10.40750	9.44177

In Fig.1 the values of $m_{\rm s}$ used in the es-TPT1 model are plotted against temperature and compared to the value of $m_{\rm f}$ used to model the fluid phases. A clear pattern is observed in which the effective length of the chains in the solid phase is larger than that in the fluid at low temperatures ($m_{\rm s} > m_{\rm f}$), a consistent result with the more-extended conformation of the molecules in the real solid phase [90]. It is interesting to see that as the temperature increases, the value of $m_{\rm s}$ tends to that of $m_{\rm f}$, and at the highest temperatures the chain length of the solid estimated in this method is found to be smaller that that used to model the fluid phases, perhaps as a result of the high-density of such states.

3. Phase behaviour

We carry out solid–liquid–vapour phase equilibrium calculations for a range of *n*-alkanes, selected by the availability of solid–fluid experimental data, and compare the two theoretical models presented: the original TPT1 model of Vega et al., as extended to the solid phase [76] in which the same number of segments is used to model the molecules in the fluid and solid phase (i.e., $m_{\rm f} = m_{\rm s}$), and the es-TPT1 model proposed in the current work in which a different number of segments is used to model the solid phase $m_{\rm f} \neq m_{\rm s}$.

In Figure 2 the melting lines are presented in $P-T$ phase diagrams, and the available experimental data [35–47] are compared to the calculations carried out with the two models. As can be seen in the figure, when the original soft-SAFT model parameters are used to treat both the fluid and solid phase (TPT1 model) little agreement is found between the calculations and the experimental data (these results are consistent with those previously presented by Vega et al. [76] for model systems). The melting lines calculated using the TPT1 model present a slope visibly smaller that that of the experiments, and are hardly seen to change as the lengths of the *n*-alkanes increase. Using the es-TPT1 model ($m_{\rm f} \neq m_{\rm s}$) leads to a marked improvement in the description of the melting lines both in terms of the slope and position, as can be expected given the procedure followed to determine the value of the

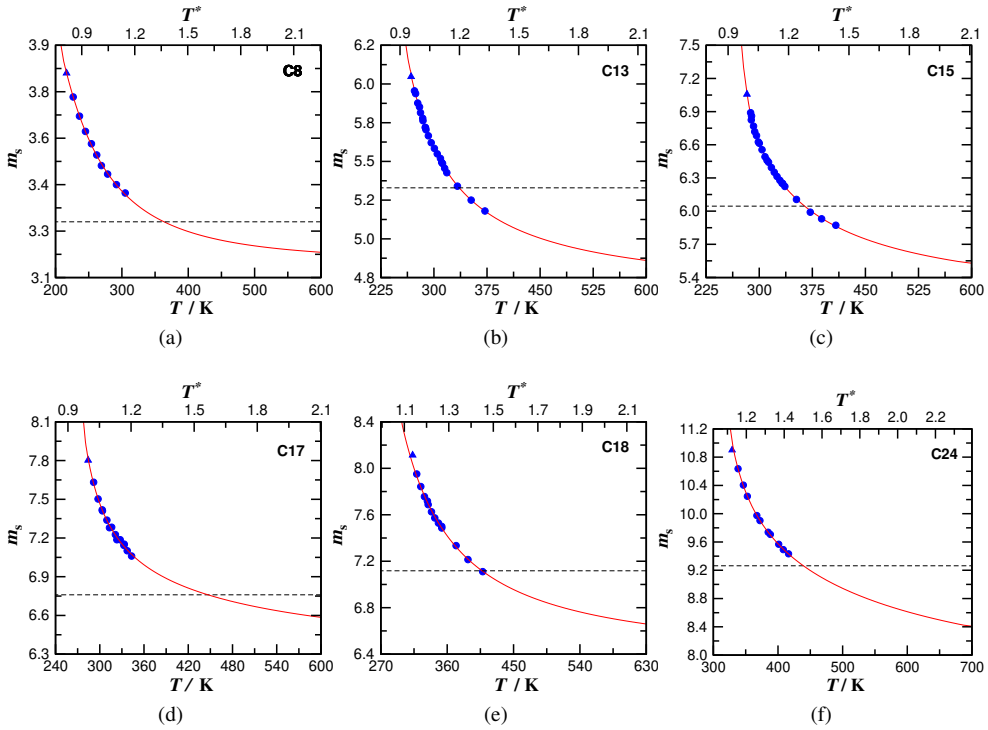


Figure 1. Number of segments m_s used to model the solid phase in the es-TPT1 model against temperature. The temperature is shown in reduced (top x-axis) and real (bottom x-axis) units. Blue circles correspond to the values of m_s obtained using eq. (13), with the corresponding fitting curves obtained from eq. (14) shown as red curves. Melting points at atmospheric pressure are indicated as triangles. The dashed lines correspond to the number of segments in the fluid the fluid phase m_f, shown for comparison.

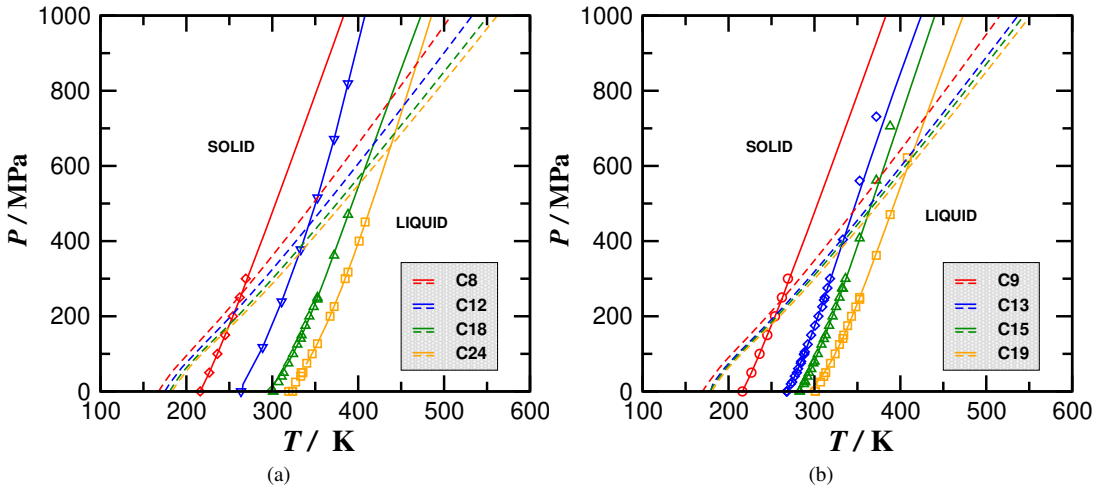


Figure 2. $P-T$ phase diagrams obtained from the models presented in Section 2 for (a) even and (b) odd n-alkanes. Continuous lines correspond to calculated melting lines using the es-TPT1 model ($m_f \neq m_s$) and dashed lines calculations with the TPT1 model ($m_f = m_s$). The symbols correspond to experimental data [35–47].

model chain length in the solid phase. In order to assess the accuracy of the es-TPT1 model, the percentage average absolute deviation %AAD of the solid–fluid equilibrium pressure is used, calculated as $\%\text{AAD} = 1/n \sum_{i=1}^{n} |(P_i^{\text{exp}} - P_i^{\text{cal}})/P_i^{\text{exp}}|$, where n is the number of data

points and P_i^{exp} and P_i^{cal} are the experimental and calculated melting pressures of point i, respectively. The calculated values of %AAD are shown in Table 3.

Table 3. Percentage verage absolute deviations %AAD of the solid–liquid melting pressures obtained using the es-TPT1 model proposed in the current work. n indicates the number of experimental points used.

n-alkane	n	T range/K	% AAD P_{melting}	Experiment
C7	7	177.15 – 225.15	0.624	[35]
C8	7	216.20 – 269.20	0.734	[35]
C9	11	219.65 – 333.15	7.111	[35, 46]
C12	26	263.65 – 388.15	0.653	[36, 41, 46]
C13	25	267.65 – 368.65	0.602	[36, 44, 46]
C15	25	282.65 – 408.15	10.03	[36, 46]
C16	12	291.10 – 343.15	0.304	[37, 40, 43, 47]
C17	16	293.35 – 349.15	0.298	[37, 39, 42, 43]
C18	16	300.95 – 416.75	0.258	[36, 46]
C24	10	323.15 – 439.65	0.333	[36, 38, 45, 46]

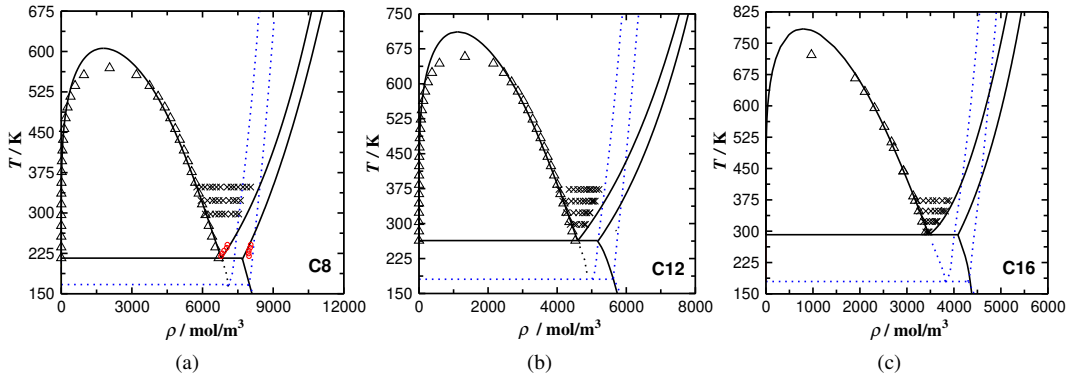


Figure 3. $T-\rho$ phase diagrams for n-octane (C8), n-dodecane (C12), and n-hexadecane (C16). The dotted blue curves and dotted blue lines correspond to calculations using the TPT1 model ($m_{\text{f}} = m_{\text{s}}$). Continuous black curves and continuous black lines correspond to calculations using the es-TPT1 model ($m_{\text{f}} \neq m_{\text{s}}$). The black triangles correspond to experimental vapour–liquid equilibrium data [91–94], the red circles to liquid–solid computer simulation results from Polson and Frenkel [90], and the crosses to single-phase liquid states [95–98].

Having confirmed the validity of the es-TPT1 model in terms of the description of the melting lines, we proceed to study the solid–liquid–vapour phase behaviour. The temperature-density ($T-\rho$) phase diagrams for n-octane, n-dodecane and n-hexadecane are presented in Figure 3. It is interesting to compare the resulting phase diagrams predicted with the two models. As the chain length increases from n-octane to n-hexadecane the vapour-liquid critical temperature increases, and the vapour–liquid envelope broadens (note the different range of the different panels in the figure). The soft-SAFT model delivers a very accurate description of the fluid-phase boundaries. In terms of the liquid–solid phase-boundary densities, these are seen to increase with temperature for each of the n-alkanes studied. Both models exhibit this trend, but the slope is clearly larger in the case of the es-TPT1 model. Although few data are available, in Figure 4 a comparison of simulation [90] and calculated saturation liquid–solid densities for n-octane can be seen more clearly. The excellent agreement obtained with the es-TPT1 model is apparent. The larger slope of the saturated liquid–solid curves that can be seen in Figure 3 leads to the prediction of higher triple temperatures in the case of our es-TPT1 model, and to reproducing the experimental trend of larger triple temperatures for larger chain lengths. We examine the prediction of the triple temperatures in more detail later.

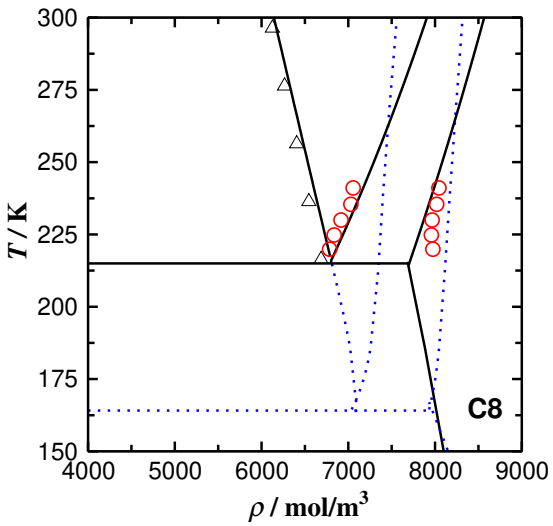


Figure 4. $T-\rho$ solid–liquid coexistence for *n*-octane. Blue dotted curves and lines are obtained using the TPT1 model ($m_f = m_s$), black continuous curves and lines correspond to the phase equilibria predicted with the es-TPT1 model ($m_f \neq m_s$). The red circles denote computer simulation results from Polson and Frenkel [90] and triangles indicate experimental VLE [92].

In terms of the available density data, single-phase experimental data in the small region between the vapour-liquid and liquid-solid phase boundaries in which the liquid is stable are also shown in Figure 3. As can be seen both the TPT1 model and the es-TPT1 predict these points as stable (with the exception of a few points in the case of *n*-octane with the phase boundaries calculated using the TPT1 model). The calculated phase boundaries with the es-TPT1 model are, however, closer to the stability boundaries suggested by the single-phase experimental data [78, 95–98].

Table 4. Triple-point temperatures in K for the set of *n*-alkanes studied in the current work. Predictions with the TPT1 ($m_f = m_s$) and es-TPT1 ($m_f \neq m_s$) models are presented. The experimental data are taken from NIST [92].

n-alkane	TPT1	es-TPT1	Experiment
C7	161.39	182.60	182.56 ± 0.03
C8	167.10	216.00	216.20 ± 0.60
C9	170.06	218.50	219.60 ± 0.50
C12	180.68	263.65	263.60 ± 0.05
C13	179.10	268.30	267.79 ± 0.01
C15	178.70	282.80	283.10 ± 0.01
C16	179.54	291.50	291.50 ± 0.10
C17	183.62	294.87	295.14 ± 0.70
C18	186.80	298.00	301.00 ± 0.30
C24	183.45	327.64	323.65 ± 0.20

In Fig. 5 $\log P - T$ representations of the phase diagrams for *n*-octane, *n*-dodecane, *n*-hexadecane and *n*-octadecane are presented in which the sublimation, vapor pressure curve and melting lines can be seen. Experimental data and calculations carried out with the TPT1 and es-TPT1 models are compared. As can be seen, excellent agreement is observed for the vapour pressure curves, in agreement with previously reported soft-SAFT calculations [64, 65], as well as for the melting line (as seen also in Figure 2) when the es-TPT1 model is used. As a result, the triple-point temperatures are predicted very accurately

using the es-TPT1 model proposed here (cf. Table 4). In contrast, the TPT1 model is seen to underestimate the value of the triple point temperature (T_{tr}) by as much as 140 K (cf. Table 4). The odd-even effect seen in many properties of the *n*-alkanes [99, 100], including the triple point temperature, is captured by the es-TPT1 model. This can be seen more clearly in Figure 6, in which the excellent agreement between the predicted triple-point temperatures using the es-TPT1 model and experiment is evident.

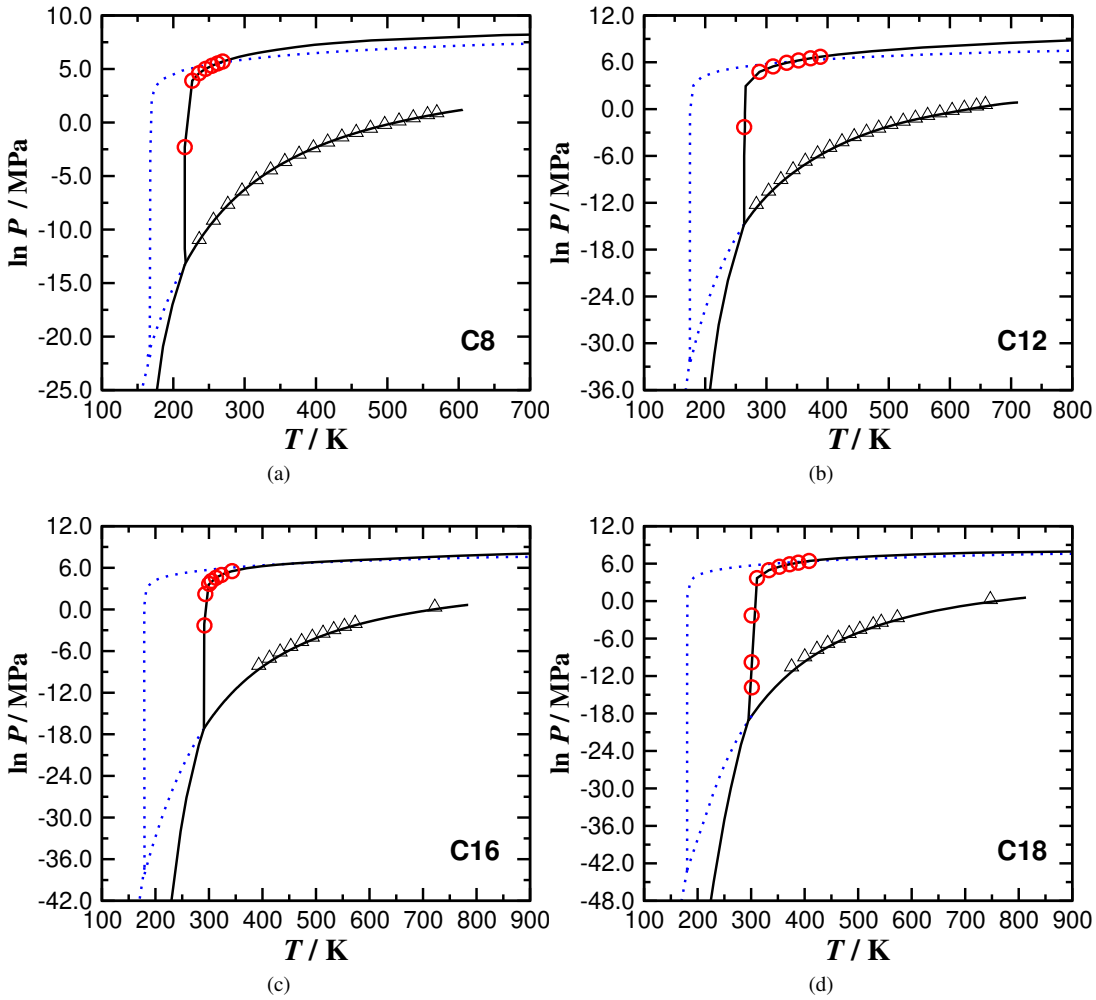


Figure 5. $\log P - T$ projections of the solid–liquid-vapour phase diagrams for *n*-octane (C8), *n*-dodecane (C12), *n*-hexadecane (C16) and *n*-octadecane (C18). The dotted blue curves correspond to calculations using the TPT1 model, and the continuous black curves to calculations using the es-TPT1 model. The symbols correspond to experimental data: black triangles for VLE [92, 95], and red circles for SLE [35–47].

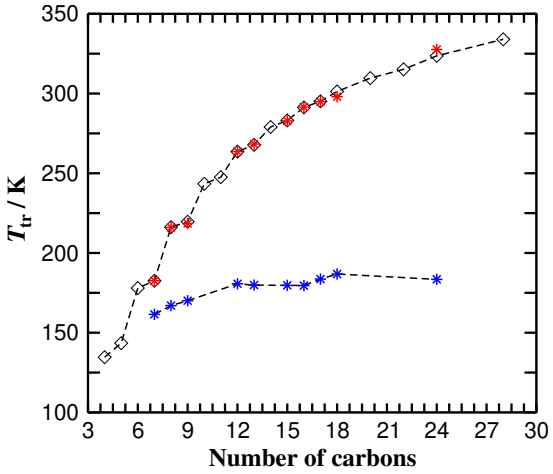


Figure 6. Predicted triple-point temperatures for the selected range of *n*-alkanes, blue and red stars correspond to TPT1 and es-TPT1 predictions, respectively. Experimental data [92] are given by open diamonds. The dashed lines are added as visual aid.

4. Conclusions

We have applied Wertheim's TPT1 framework to study the solid−fluid equilibrium of several *n*-alkanes modelled as chains of freely-jointed tangent LJ segments. A model has been proposed in which the chain length used to model the solid phase is different to that used to model the fluid phase; we refer to this model as es-TPT1. The non-existence of a critical point between solid and fluid phases permits the use of different models to treat these phases. The effective chain length used in the solid phase is determined by comparison to experimental melting-pressure data. Furthermore, the resulting model leads to significant improvement compared to the TPT1 model in the calculated phase diagrams of the *n*-alkanes considered, which are now found to be in very good agreement with experiment, including the accurate prediction of the triple point temperatures. This is in contrast with the original model in which the same number of segments in used to treat the fluid and solid phases [76], which leads to the overestimation of the stability of the fluid phases. The new values proposed for the number of segments m_s used to model the solid phase are consistent with the expected physical behaviour of extended *n*-alkane chain molecules at low temperatures. In future work we will address the extension of this approach to study the phase behaviour of mixtures including solid and fluid phases.

Acknowledgement(s)

We acknowledge support from the University of Guanajuato (CIIC 151/2022) and CONACYT (México) for a PhD scholarship (VRC). Amparo Galindo acknowledges support from the Royal Academy of Engineering and Eli Lilly and Company for support of a Research Chair (Grant RCSRF18193). We also gratefully acknowledge Luis Alcázar-Vara and Eduardo Buenrostro-González (Instituto Mexicano del Petróleo, México) for very usefull discussions and information about experimental data. .

References

[1] K.S. Pedersen, P.L. Christensen, J.A. Shaikh and P.L. Christensen, *Phase behavior of petroleum reservoir fluids*, 1st ed. (CRC Press, Boca Raton, 2006), p. 422.

[2] M. Freund, R. Csikós, S. Keszthelyi and G. Mózes, *Paraffin products*, 1st ed. (Elsevier, New York, 1983).

[3] D.W. Jennings and K. Weispfennig, Fluid Phase Equilibria **227**, 27 (2005).

[4] J.A.P. Coutinho, B. Edmonds, T. Moorwood, R. Szczepanski and X. Zhang, Energy & Fuels **20**, 1081 (2006).

[5] L.A. Alcazar-Vara and E. Buenrostro-Gonzalez, Fuel Processing Technology **92**, 2366 (2011).

[6] L.A. Alcazar-Vara, J.A. Garcia-Martinez and E. Buenrostro-Gonzalez, Fuel **93**, 200 (2012).

[7] H. Peng, D. Zhang, X. Ling, Y. Li, Y. Wang, Q. Yu, X. She, Y. Li and Y. Ding, Energy & Fuels **32**, 7262 (2018).

[8] S. Kahwaji, M.B. Johnson, A.C. Kheirabadi, D. Groulx and M.A. White, Energy **162**, 1169 (2018).

[9] K.D. Papavasileiou, L.D. Peristeras, A. Bick and I.G. Economou, The Journal of Physical Chemistry B **123**, 6229 (2019).

[10] 1, Proteins **11**, 281 (1991).

[11] J.N. Israelachvili, *Intermolecular and Surface Forces*, 3rd ed. (Academic Press, USA, 2011), p. 501.

[12] D. Myers, *Surfaces, Interfaces, and Colloids: Principles and Applications*, 2nd ed. (Wiley, New York, 2002).

[13] H. Huang, M. Burghardt, A. Schuster, J. Leide, I. Lara and M. Riederer, J. of Agricultural and Food Chemistry **65**, 8790 (2017).

[14] A. Richardson, R. Franke, G. Kerstiens, M. Jarvis, L. Schreiber and W. Fricke, Planta **222**, 472 (2005).

[15] C.L. Thomas, B. Jansen, E.E. van Loon and G.L.B. Wiesenberg, Soil **7**, 785 (2021).

[16] P.A. Monson and D.A. Kofke, Adv. Chem. Phys **115**, 113 (2000).

[17] A.P. Malanoski and P.A. Monson, J. Chem. Phys. **107**, 6899 (1997).

[18] A.P. Malanoski and P.A. Monson, J. Chem. Phys. **110**, 664 (1997).

[19] J.M. Polson and D. Frenkel, J. Chem. Phys. **109**, 318 (1998).

[20] P.K. Weiner and P.A. Kollman, J. Comput. Chem. **2**, 287 (1981).

[21] B.R. Brooks, R.E. Bruccoleri, B.D. Olafson, D.J. States, S.A. Swaminathan, and M. Karplus, J. Comput. Chem. **4**, 187 (1983).

[22] B.R. Brooks, C.L.B. III, J. A. D. Mackerell, L. Nilsson, R.J. Petrella, B. Roux, Y. Won, G. Archontis, C. Bartels, A.C. S. Boresch, L. Caves, Q. Cui, A.R. Dinner, M. Feig, S. Fischer, J. Gao, M. Hodoscek, W. Im, K. Kuczera, T. Lazaridis, J. Ma, V. Ovchinnikov, E. Paci, R.W. Pastor, C.B. Post, J.Z. Pu, M. Schaefer, B. Tidor, R.M. Venable, H.L. Woodcock, X. Wu, W. Yang, D.M. York and M. Karplus, J. Comput. Chem. **20**, 1545 (2009).

[23] W.F. van Gunsteren, X. Daura and A.E. Mark, J. Comput. Chem. **19**, 535 (1998).

[24] W.L. Jorgensen, J.D. Madura and C.J. Swenson, J. Am. Chem. Soc. **106**, 6638 (1984).

[25] W.L. Jorgensen, D.S. Maxwell and J. TiradoRives, J. Am. Chem. Soc. **118**, 11225 (1996).

[26] M. Martin and J. Siepmann, J. Chem. Phys. **102**, 2559 (1998).

[27] J. Alejandre, D.J. Tildesley and G.A. Chapela, Mol. Phys. **85**, 651 (1995).

[28] B.Chen, J.I. Siepmann, K.J. Oh and M.L. Klein, J. Chem. Phys. **116**, 4317 (2002).

[29] S.O. Nielsen, C.F. Lopez, G. Srinivas and M.L. Klein, J. Chem. Phys. **119**, 7043 (2003).

[30] J. Pàmies, C. McCabe, P. Cummings and L.F. Vega, Mol. Simul. **29**, 463 (2003).

[31] M.A. Amat and G.C. Rutledge, J. Chem. Phys. **132**, 114704 (2010).

[32] S.W.I. Siu, K. Pluhackova and R.A. Böckmann, J. Chem. Theory Comput. **8**, 1459 (2012).

[33] W.L. Jorgensen, D.S. Maxwell and J. Tirado-Rives, J. Am. Chem. Soc. **118**, 11225 (1996).

[34] S.A. Burrows, I. Korotkin, S.K. Smoukov, E. Boek and S. Karabasov, J. Phys. Chem. B **125**, 5145 (2021).

[35] A. Würflinger, Berichte Der Bunsengesellschaft Für Phys. Chemie **79**, 1195 (1975).

[36] A. Würflinger and G. Schneider, Berichte Der Bunsengesellschaft Für Phys. Chemie **77**, 121

(1973).
[37] A. Würflinger and M. Sandmann, Zeitschrift fur Naturforschung - Section A Journal of Physical Sciences **55**, 533 (2000).
[38] G. Höhne and K. Blankenhorn, Thermochimica Acta **238**, 351 (1994).
[39] J. Pauly, J. Coutinho and J. Daridon, Fluid Phase Equilib. **255**, 193 (2007).
[40] P. Morawski, J.A.P. Coutinho and U. Domańska, Fluid Phase Equilibria **230**, 72 (2005).
[41] U. Domańska and P. Morawski, J. Chem. Thermodynamics **37**, 1276 (2005).
[42] U. Domańska and P. Morawski, J. Chem. Eng. Data **50**, 1073 (2005).
[43] Y. Tanaka and M. Kawakami, Fluid Phase Equilib. **125**, 103 (1996).
[44] J.L. Daridon, J. Pauly and M. Milhet, Phys. Chem. Chem. Phys. **4**, 4458 (2002).
[45] J.J.B. Machado, T.W. de Loos, E.C. Ihmels, K. Fischer and J. Gmehling, The Journal of Chemical Thermodynamics **40**, 1632 (2008).
[46] R.R. Nelson, W. Webb and J.A. Dixon, J. Chem. Phys. **33**, 1756 (1960).
[47] M. Milhet, J. Pauly, J.A.P. Coutinho, M. Dirand and J.L. Daridon, Fluid Phase Equilibria **235**, 173 (2005).
[48] M.L. Huggins, J. Chem. Phys. **9**, 440 (1941).
[49] P.J. Flory, J. Chem. Phys. **9**, 660 (1942).
[50] R. Dickman and C.K. Hall, J. Chem. Phys. **85**, 4108 (1986).
[51] K.G. Honnell and C.K. Hall, J. Chem. Phys. **90**, 1841 (1989).
[52] J.A.P. Coutinho, S.I. Andersen and E.H. Stenby, Fluid Phase Equilibria **103**, 23 (1994).
[53] J.A.P. Coutinho, S.I. Andersen and E.H. Stenby, Fluid Phase Equilibria **117**, 138 (1996).
[54] M.S. Wertheim, J. Stat. Phys. **35**, 19 (1984).
[55] M.S. Wertheim, J. Stat. Phys. **35**, 35 (1984).
[56] M.S. Wertheim, J. Stat. Phys. **42**, 459 (1986).
[57] M.S. Wertheim, J. Stat. Phys. **42**, 477 (1986).
[58] M.S. Wertheim, J. Chem. Phys. **87**, 7323 (1987).
[59] M.S. Wertheim, J. Chem. Phys. **85**, 2929 (1986).
[60] W.G. Chapman, G. Jackson and K.E. Gubbins, Fluid Phase Equilibria **52**, 31 (1989).
[61] W.G. Chapman, G. Jackson, K.E. Gubbins and M. Radosz, Ind. Eng. Chem. Res. **29**, 1709 (1990).
[62] A. Gil-Villegas, A. Galindo, P.J. Whitehead, S.J. Mills, G. Jackson and A.N. Burgess, J. Chem. Phys. **106**, 4168 (1997).
[63] A. Galindo, L.A. Davies, A. Gil-Villegas and G. Jackson, Mol. Phys. **93**, 241 (1998).
[64] F.J. Blas and L.F. Vega, Mol. Phys. **92**, 135 (1997).
[65] F.J. Blas and L.F. Vega, Ind. Eng. Chem. Res. **37**, 660 (1998).
[66] J. Gross and G. Sadowski, Ind. Eng. Chem. Res. **41**, 1084 (2002).
[67] T. Lafitte, A. Apostolakou, C. Avendaño, A. Galindo, C.S. Adjiman, E.A. Müller and G. Jackson1, J. Chem. Phys. **139**, 154504 (2013).
[68] E.A. Müller and K.E. Gubbins, Ind. Eng. Chem. Res. **40**, 2193 (2001).
[69] I.G. Economou, Ind. Eng. Chem. Res. **41**, 953 (2002).
[70] P. Paricaud, A. Galindo and G. Jackson, Fluid Phase Equilibria **194**, 87 (2002).
[71] S.P. Tan, H. Adidharma and M. Radosz, Ind. Eng. Chem. Res. **47**, 8063 (2008).
[72] G. Kontogeorgis and G.K. Folas, *Thermodynamic Models For Industrial Applications* (, , 2010).
[73] C. McCabe and A. Galindo, *SAFT associating fluids and fluid mixtures, in Applied Thermodynamics of Fluids*, 1st ed. (The Royal Society of Chemistry,, UK, 2010), p. 215.
[74] J.K. Johnson, E.A. Müller and K.E. Gubbins, J. Phys. Chem. **98**, 6413 (1994).
[75] C. Vega and L.G. MacDowell, J. Chem. Phys. **114**, 10411 (2001).
[76] C. Vega, F.J. Blas and A. Galindo, J. Chem. Phys. **116**, 17 (2002).
[77] M.A. van der Hoef, J. Chem. Phys. **113**, 8142 (2000).
[78] D.L. Morgan and R. Kobayashi, Fluid Phase Equilibria **63**, 317 (1991).
[79] F.J. Blas, A. Galindo and C. Vega, Mol. Phys. **101**, 449 (2003).
[80] F.J. Blas, E. Sanz, A. Galindo and C. Vega, J. Chem. Phys. **119**, 10958 (2003).
[81] A. Galindo, C. Vega, E. Sanz, L.G. MacDowell, E. de Miguel and F.J. Blas, J. Chem. Phys. **120**, 3957 (2004).

[82] Y. Zhou and G. Stell, J. Chem. Phys. **96**, 1507 (1992).
[83] A. Galindo, P.J. Whitehead, G. Jackson and A.N. Burgess, J. Phys. Chem **100**, 6781 (1996).
[84] J.K. Johnson, J.A. Zollweg and K.E. Gubbins, Mol. Phys. **78**, 591 (1993).
[85] J.S. Rowlinson and F.L. Swinton, *Liquids and Liquid Mixtures*, 3rd ed. (Butterworth Scientific, UK, 1982), p. 59.
[86] W.H. Press, S.A. Teukolsky, W.T. Vetterling and B.P. Flannery, *Numerical Recipes: The Art of the Scientific Computing*, 3rd ed. (Cambridge University Press, New York, 2007).
[87] J.C. Pàmies and L.F. Vega, Ind. Eng. Chem. Res. **40**, 2532 (2001).
[88] F. Llovell and L.F. Vega, J. Chem. Phys. **110**, 1350 (2006).
[89] F. del Río and A. Gil-Villegas, Molecular Physics **77**, 223 (1992).
[90] J.M. Polson and D. Frenkel, J. Chem. Phys. **111**, 22 (1999).
[91] R.H. Perry and D.W. Green, *Perry's Chemical Engineers' Handbook*, eighth ed. (McGraw-Hill, Mexico City, 2008).
[92] National Institutes of Standards and Technology, Physics Laboratory, Physical Reference Base 2023, July. <http://physics.nist.gov./PhysRefData/contents.html>.
[93] Gesellschaft für Chemische Technik und Biotechnologie e.V. . <https://dechema.de/en/detherm.html>.
[94] F.D. Rossini, K.S. Pitzer, W.J. Taylor, J.P. Ebert, J.E. Kilpatrick, C. W.Beckett, M..G. Williams and H. G.Werner, *Selected Values of Properties of Hydrocarbons and Related Compounds* (American Petroleum Institue, Research Project 44, Dept. of Commerce, National Bureau of Standards, USA, 1995).
[95] D.L. Morgan and R. Kobayashi, Fluid Phase Equilibria **97**, 211 (1994).
[96] J.H. Dymond, J.H. Robertson and J.D. Isdale, J. Chem. Thermodynamics **14**, 51 (1982).
[97] S. Outcalt, A. Laesecke and J.F. Tara, J. Chem. Thermodynamics **42**, 700 (2010).
[98] S. Dutour, J.L. Daridon and B. Lagourette, International Journal of Thermophysics **21**, 173 (2000).
[99] W.F. Seyer, R.F. Patterson and J.L. Keays, Journal of the American Chemical Society **66** (2), 179–182 (1944).
[100] R. Boese, H.C. Weiss and D. Bläser, Angewandte Chemie International Edition **38** (7), 988–992 (1999).